# Coeval Decline of Biological Productivity and Bottom-water Oxygenation in EEP Ocean Recorded by Magnetofossils during the Antarctic Glaciation

Dunfan Wang[1], Yang Lu[1], Congcong Gai[1], Peiling Xie[1], Yutong Jiang[1], Zeheng Ruan[1], Qingsong Liu[1,2*]

[1] Centre for Marine Magnetism (CM$^2$), Department of Ocean Science and Engineering, Southern University of Science and Technology, Shenzhen 518055, China.

[2] Southern Marine Science and Engineering Guangdong Laboratory (Guangzhou), 511458, China.

Corresponding author: Qingsong Liu, qsliu@sustech.edu.cn

**Key Points:**

- Magnetofossil is a valuable proxy to trace the past dust fertilization and bottom-water oxygenation in eastern equatorial Pacific (EEP) Ocean
- The EEP biological productivity and deep-ocean ventilation coeval declined during the Antarctic glaciation expansion
- Deep-ocean ventilation primarily controlled the $CO_2$ outgassing in the EEP, with superimposed biological pump playing a stabilizing role

**Abstract**

The biological pump and deep-ocean ventilation in eastern equatorial Pacific (EEP) Ocean are thought to play a crucial role in cases of global $CO_2$ change. However, the integral role of these two processes in regulating atmospheric $CO_2$ perturbations over major climate transitions are still unknown. Here, we present the magnetofossil record in EEP sediments from Sites 1333 and 1218 across the Eocene-Oligocene Transition (EOT) when the major ice-sheet was first established on Antarctica. We find that the EEP dust fertilization and bottom-water oxygenation were well co-archived by magnetofossil in characteristics of abundance and morphology, respectively. Our observations show a coeval decline of EEP biological productivity and deep-ocean ventilation during the Antarctic glacial expansion, and suggest that the reduced deep-ocean ventilation contributed to the global $CO_2$ decline across the EOT, whereas the superimposed biological pump action provided a negative (stabilizing) feedback in the meantime.

**Plain Language Summary**

The integral role of the eastern equatorial Pacific (EEP) Ocean to global $CO_2$ perturbations over major climate transition remains debated. Here, we investigated the combined influences of EEP dust fertilization and deep-ocean ventilation on the later Eocene to early Miocene global $CO_2$ decline using a novel biological magnetofossil proxy. We find that the magnetofossil is a valuable palaeoenvironmental indicator whose abundance and morphology strongly linked to the dust inputs and the deep-ocean oxygenation, respectivily. Based on these records, we proposed that the deep-ocean ventilation primarily controlled the later Eocene to early Miocene $CO_2$ decline in EEP Ocean, and in the meantime, however, the superimposed biological pump action played a negative and stabilizing role.

## 1. Introduction

The eastern equatorial Pacific (EEP) Ocean is one of the major iron-limited high-nutrient, low-chlorophyll (HNLC) regions and it plays a crucial role in global climate changes and carbon cycles (Martin, 1990; Erhardt, 2017). The EEP surface iron fertilization and deep-ocean ventilation are two principal processes that contribute to the case of global atmospheric $CO_2$ perturbation (Murray et al., 2012; Marcantonio et al., 2020). Today, the EEP Ocean mainly acts as a net $CO_2$ source to atmosphere because the elevated ventilation promotes the outgassing of the respired carbon pool stored in deep ocean (Takahashi et al., 2009). However, it could be a net $CO_2$ sink in the geological past if the biological pump enhanced by more dust supply to augment the $CO_2$ remove from the atmosphere (Loveley et al., 2017). Therefore, efficiency of iron fertilization and changes in ocean ventilation together controlled the sea-air $CO_2$ budget in this region.

Costa et al. (2016) has claimed that there was no iron fertilization in the EEP ocean during the Last Glacial Period (LGP) because the subsurface major nutrient concentrations were lower in the central equatorial Pacific during that time. They, therefore, concluded that large nutrient was consumed by dust fertilization in subantarctic zone of Southern Ocean during the LGP, and that made the EEP subsurface nutrients depleted and ultimately lowed the iron fertilization in EEP. In fact, besides the oceanic productivity, the Pacific deep-ocean ventilation is also substantially incked to the Antarctic climate states, which would substantially account for the deep ocean respired carbon pool variations and resultant global $CO_2$ cycles (Martinez-Garcia et al., 2014). Understanding the EEP Ocean fertilization is challenging now (Lyle, 2008; Jacobel et al., 2019). Although many attentions have been focused on there to investigate the relationship between dust fertilization and carbon cycles, arguments both for and against it are reported (Winckler et al., 2016; Costa et al., 2016; Loveley et al., 2017). Meanwhile, the associated role of deep-ocean ventilation is rarely considered.

Valuable paleoenvironmental indicators that could co-archive surface fertilization and bottom-water oxygenation variations at the same time provide a new insight in understanding the integral role of the EEP in regulating the atmospheric $CO_2$. Magnetotactic bacteria (MTB) inhabiting near the sediment oxic-anoxic transition zone (OATZ) could intracellularly synthesize magnetite with iron and organic matter supply (Amoret al., 2020). Their nanomagnetic remains will be buried in sediment when they die and fossilized to be magnetofossils (Kirschvink & Chang, 1984). Magnetofossils are now recognized to be widespread in pelagic marine sediments and regarded as a well-preserved biomarker (Kopp & Kirschvink, 2008; Roberts et al., 2013). Moreover, its abundance as well as morphology are sensitive to environmental changes such as iron supply, carbon export production, and bottom water oxygenation (Chang et al., 2018; He & Pan, 2020). That makes magnetofossil competent as a proxy to archive combined roles of surface dust fertilization and deep-sea ventilation to global $CO_2$ perturbation during global climate changes.

Here, we present records of dust input, biological productivity, and bottom water oxygenation from two cores of International Ocean Discovery Program Sites 1333 and 1218, which were located in the present-day EEP HNLC region from the late Eocene to early Miocene. (Figure.1). By using magnetofossil abundance and morphology signatures as the indicators of export productivity and bottom-water oxygenation, respectively, we explored the combined roles of EEP dust fertilization and deep-ocean ventilation in regulating the global $CO_2$ perturbation during the first build-up of major Antarctic glaciation across the Eocene-Oligocene Transition (EOT).

## 2. Methods

We measured first-order reversal curves (FORCs) to detect magnetofossils in EEP sediments (Robert et al., 2000). Hysteresis loops and backfield demagnetization curves were measured to calculate the coercivity ($B_c$) and remanence coercivity ($B_{cr}$) for bulk sediments. Isothermal remanent magnetizations (IRM) curves were decomposed into different magnetic components using the approach of Kruiver et al. (2001). Transmission electron microscope (TEM) observation was subjected to samples after magnetic extraction for magnetofossil morphologies identification and statistical analysis. $ARM_{@20\ mT}$ (anhysteretic remanent magnetization after alternating field demagnetization at 20 mT) was measured to estimate the sediment magnetofossil abundance (e.g. Robert et al., 2011). Aeolian dust (using the concentration of hematite and goethite, expressed as $Rel_{Hm+Gt}$), primary production (using opal), and export productivity (using biogenic "excess" Ba, expressed as xsBa) were also measured for bulk sediments to quantify the relationship between dust supply and export productivity (Detailed methods see supplementary Text S1).

## 3. Results

### *3.1. FORC diagram and IRM unmixing results*

FORC diagrams (Figure. 2a-c) show the same characteristics featured by a sharp central ridge along $B_u = 0$ axis, which indicates the dominance of non-interacting single domain magnetofossils (Egli et al., 2010). IRM unmixing results (Figure. 2d-f) indicate that studied sediments contain four magnetic components: Aeolian magnetic materials with low and high coercivities (components 1 and 4), biogenic soft (BS) and biogenic hard (BH) magnetite (components 2 and 3). Fitted IRM parameters also indicate that aeolian dust components have relatively consistent coercivity and lower abundance in studied samples, and the percentage content of BH magnetofossil increased across the EOT at ~34 Ma. These magnetic results provide strong evidence of magnetofossil occurrences within the EEP sediments and it is dominated in each sample with low dispersion (Supplementary Table S1).

*3.2. Magnetofossil morphological characteristics and abundance variations*

Magnetofossils with different morphologies including cuboctahedron, prism, and bullet are directly identified from TEM observations and further distinguished by the shape factor of axial ration (width/length, W/L) (Figure. 2g–l). Refer to the size distribution and classification method of Kopp and Kirschvink (2008), we divide magnetofossils into two categories with high ($W/L < 0.6$) and lower ($0.6 < W/L < 1$) anisotropy, which correspond to the BH and BS magnetite isolated by the IRM decomposition, respectively (Lascu & Plank, 2013; He & Pan, 2020). A statistical analysis based on more than 4,000 magnetofossil crystals from EEP sediments shows that the bullet-shaped magnetofossil proportion increased after the EOT with the Antarctic glaciation expansion (Figure. 2i).

The aeolian dust input ($Rel_{Hm+Gt}$), biological productivity (opal, xsBa) and magnetofossils abundance ($ARM_{@20\ mT}$) dropped sharply across the EOT, and then gradually returned to pre-EOT values since ~26 Ma (Figure. 3a-d), which coincides with the onset of Antarctic glaciation expansion at the EOT and late Oligocene Antarctic ice-sheet reduction (Zachos et al., 2001, Rohling et al., 2021). The bulk sediment $B_c$, and $B_{cr}$ gradually increased after the EOT and nearly remain at the same level after ~26 Ma, which have the same trend with the later Eocene to early Miocene $CO_2$ decline (Figure. 3e-g).

## 4 Discussion

### *4.1. Impacts of EEP dust fertilization and biological pump action on global $CO_2$ variation*

Dust production, emission, and deposition are closely linked to Earth's climate state (Rea et al., 1998). We observe a prominent dust reduction across the EOT followed by a gradual return to pre-EOT values at ~26 Ma with the ice-sheet retreat (Figure. 3a), which suggests that the Antarctic ice-sheet expansion had a vital impact on source environment and principally controlled the EEP dust supply. The coherent variations of opal and xsBa coincide with EEP dust supply demonstrate that dust dissolution released iron and fueled the EEP biological productivity over the 40-18 Ma interval, which agrees with the suggestion of dust input from land to sea is the major external iron source to stimulate the marine biological activity (Lovevely et al., 2017; Tagliabue et al., 2017). Roberts et al. (2011) has demonstrated that MTB productivity is limited by the organic carbon and iron supply because they require dissolved iron and organic matter to biomineralize magnetite, and magnetofossil abundance, therefore, could be used as a valuable productivity proxy of carbon to seafloor. In our study, the variations of magnetofossil abundance are well-relate to opal and xsBa. This result futher demonstrates that magnetofossil abundance is a valuable export productivity proxy in iron limited environment and it could provide a new insight into the understanding of relationship between dust fertilization and carbon burial over geological timescales, which is controversial in EEP regions (Lyle, 2008; Jacobel et al., 2019).

The EOT was a major climate change during which the Earth transitioned from a largely ice-free greenhouse to an icehouse world with sharply reduced atmospheric $CO_2$ (Goldner et al., 2014; Hutchinson et al., 2021). Based on the high-resolution record of marine barite accumulation rates, Erhardt et al. (2013) claimed that the EEP productivity was reduced after the EOT and the biological pump did not contribute to the carbon sequestration during global cooling across the

EOT. Our magnetofossil record show that the EEP biological pump was weakened with the global $CO_2$ decline during the ice-sheet expansion (~34-26 Ma), and slightly intensified after ~26 Ma with the ice-sheet gradually retreat. This opposite trend suggests that the EEP dust fertilization and biological pump had no contribution to the global $CO_2$ decline across the EOT, and it, in return, played a negative and stabilizing role to the global $CO_2$ change. It has been suggested that sea-level drop across the EOT and sedimentary pyrite oxidation may had constituted a climate stabilizing mechanism during the Antarctic glaciation advance (Torres et al., 2014; Yao et al., 2021). Our observation indicates that the EEP biological pump additionally contributed to that stabilizing mechanism via weakening the capacity of carbon sequestration during that time with global cooling.

*4.2. The response of deep-ocean ventilation to the Antarctic ice-sheets expansion*

Laboratory-controlled MTB culturing experiments demonstrated that the magnetofossil morphology is strongly depended on the microenvironmental oxygen content (Faivre & Schüler, 2008; Li & Pan, 2012; Katzmann et al., 2013). From example, the isotropic magnetofossil predominates in relatively oxidized conditions whereas the anisotropic magnetofossil generally formed under lower oxygen conditions, and have higher coercivity. Moreover, Previous studies of different geological magnetofossil records show that the proportion of bullet-shaped magnetofossil was commonly increased in less oxic conditions (Usui et al., 2017; Yamazaki et al., 2019). Therefore, magnetofossil morphology combined with the corresponding magnetic properties (e.g. coercivity) are often used as a paleoredox proxy to reconstruct the deep-sea oxygenation (Chang et al., 2018). Especially the high ratio of bullet-shaped magnetofossils to the other morphologies has been regarded as a signal of the less oxygen (Yamazaki & Kawahata, 1998).

Our TEM observation results show that the proportion of bullet-shaped magnetofossils increased after the EOT, which is exactly identical to the IRM unmixing result that the proportion of BH magnetite increased during the Antarctic glaciation (Supplementary Table S1). Given that biogenic magnetofossils dominated magnetic mineral components and dust materials have relatively consistent coercivity and low abundance for all studied samples, we conclude that the bulk $B_{cr}$ and $B_c$ can mainly reflect the average coercivity variation of sedimentary magnetofossils in our study. The increased post-EOT $B_{cr}$ and $B_c$ correspond to the bloom of bullet-shaped magnetofossil which has strong anisotropy and high coercivity (Figure. 3e-f), suggesting that the EEP deep ocean became less oxic after the Antarctic glaciation build-up across the EOT.

Low oxygenation can be caused by enhanced surface biological productivity which would lead to more organic carbon (OC) supply to the seafloor, and/or reduced deep-ocean ventilation with stratified conditions. Our records show that the biological productivity was abruptly declined after the EOT (Figure. 3a-d), suggesting that low oxygenation was not the result of OC supply and they, therefore, support the interpretation of the EEP deep-ocean ventilation reduced during the Antarctic ice-sheet expansion. Previous studies report that the EEP deep-ocean ventilation was declined during the glacial period and it would store more respired carbon in the deep Pacific glacial ocean (Bradtmiller et al., 2010; Jacobel et al., 2017; Loveley et al., 2017). Our records agree with this idea as the period of reduced deep-ocean ventilation was consistent with the low atmospheric $CO_2$ (Figure. 3e-g). With the Antarctic glaciation expansion, the larger ice cap may block up the gases exchange and make the deep ocean more hermetical which would substantially decrease the deep-water oxygenation after the EOT (Figure. 4).

Palaeoclimate reconstructions and modelling results suggest that the Southern Ocean intermediate water and Antarctic bottom water had developed during the early Oligocene, and the

Antarctic ice-sheet growth would enhance the northward transportation of Antarctic intermediate water and facilitate the formation of Antarctic bottom water (Katz et al., 2011; Goldner et al., 2014). That is, although the Antarctic glaciation could intensify cold water circulation, it probably just invigorated the intermediate water transfer and had less impact on the deep-ocean water circulation and upwelling. This is supported by the increased benthic foraminifer accumulation rate and the gradual shoaling of thermocline at the Eocene-Oligocene boundary (Coxall et al., 2011; Moore et al., 2014), because only a large amount of food-carried bottom-water was formed, could the benthic foraminifera be flourished when the export production was reduced, and it also would lead to a gradual shoaling of thermocline in EEP Ocean. Massive bottom-water formed in the glacial Pacific Ocean and accordingly stored more carbon in the deep sea, which support the suggestion of there would be an increased respired carbon pool in the glacial Pacific Ocean, and huge carbon would be trapped in the deep sea during glacial periods (Bradtmiller et al., 2010).

## 5 Conclusions

Our TEM analyses and magnetic results consistently indicate that magnetic nanoparticles within the eastern equatorial Pacific (EEP) sediments from Sites 1333 and 1218 are mainly magnetofossils, and they both show clear trends: magnetofossil abundance declined at the Antarctic glaciation onset across the EOT and gradually returned at ~26 Ma with the ice-sheet retreat, the morphology-depend coercivity increased after the EOT and appeared a consistent trend with global $CO_2$ decline. These results jointly reveal a coeval decline of biological productivity and bottom-water oxygenation in the EEP Ocean during the Antarctic glaciation expansion. The reduced bottom-water oxygenation associated with low atmospheric $CO_2$ indicate that a huger respired carbon pool probably formed in the deep Pacific glacial ocean. These observations suggest that the deep-ocean ventilation principally controlled the $CO_2$ outgassing in EEP regions, with superimposed biological pump action providing a negative and stabilizing feedback in the meantime.

## Acknowledgments

This study was supported by the National Natural Science Foundation of China (92158208, 41874078), the opening foundation (SSKP202101) of the Shanghai Sheshan National Geophysical Observatory, Shanghai, China, and the Shenzhen Science and Technology Program (KQTD20170810111725321), the Special Funds for "Climbing program" (pdjh2022c0030 and pdjh2021c0024), and International Ocean Discovery Program. We thank $CM^2$ members for discussions.

## Data Availability Statement

The data in this study are included in the supporting information and uploaded to Data repository.

## References

Amor, M., Mathon, F. P., Monteil, C. L., Busigny, V., & Lefevre, C. T. (2020). Iron-biomineralizing organelle in magnetotactic bacteria: function, synthesis and preservation in ancient rock samples. *Environmental. Microbiology,* 22, 3611–3632.

Bradtmiller, L. I., Anderson, R. F., Sachs, J. P., & Fleisher, M. Q. (2010). A deeper respired carbon pool in the glacial equatorial Pacific Ocean. *Earth and Planetary Science Letters,* 299(3-4), 417-425.

Chang, L., Harrison, R., Zeng, F., Berndt, T. A., Roberts, A. P., Heslop, D., & Zhao, X. (2018). Coupled microbial bloom and oxygenation decline recorded by magnetofossils during the Palaeocene–Eocene Thermal Maximum. *Nature Communications,* 9:4007.

Coxall, H. K., & Wilson, P. A. (2011). Early Oligocene glaciation and productivity in the eastern equatorial Pacific: Insights into global carbon cycling, *Paleoceanography,* 26, PA2221. https://doi.org/10.1029/2010PA002021.

Costa, K. M., McManus, J. F., Anderson, R. F., Ren, H., Sigman, D. M., Winckler, G., Fleisher, M.Q., Marcantonio, F., & Ravelo, A.C. (2016). No iron fertilization in the equatorial Pacific Ocean during the last ice age. *Nature,* 529, 519-22. https://doi.org/10.1038/nature16453

Egli, R., Chen, A. P., Winklhofer, M., Kodama, K. P., & Horng, C. S. (2010). Detection of noninteracting single domain particles using first-order reversal curve diagrams. *Geochemistry, Geophysics, Geosystems,* 11, Q01Z11.

Erhardt, A. M., Palike, H., & Paytan, A. (2013). High-resolution record of export production in the eastern equatorial Pacific across the Eocene-Oligocene transition and relationships to global climatic records. *Paleoceanography,* 28, 130–142.

Erhardt, A.M. (2017). Palaeoceanography: tropical ties. *Nature Geoscience,* 10, 714-715. https://doi.org/10.1038/ngeo3025

Faivre, D., & Schüler, D. (2008). Magnetotactic bacteria and magnetosomes. *Chemical Reviews,* 108, 4875–4898.

Goldner, A., Herold, N., & Huber, M. (2014). Antarctic glaciation caused ocean circulation changes at the Eocene–Oligocene transition. *Nature,* 511, 574–577.

He, K., & Pan, Y. (2020). Magnetofossil abundance and diversity as paleoenvironmental proxies: A case study from southwest Iberian margin sediments. *Geophysical Research Letters,* 47, e2020GL087165. https://doi. org/10.1029/2020GL087165

Hutchinson, D. K., Coxall, H. K., Lunt, D. J., Steinthorsdottir, M., & Zhang, Z. (2021). The Eocene–Oligocene transition: a review of marine and terrestrial proxy data, models and model–data comparisons. *Climate of the past,* 17, 269–315.

Jacobel, A. W., McManus, J. F., Anderson, R. F., & Winckler, G. (2017). Repeated storage of respired carbon in the equatorial Pacific Ocean over the last three glacial cycles. *Nature Communications,* 8(1727).

Jacobel, A. W., Anderson, R. F., Winckler, G., Costa, K. M., Gottschalk, J., Middleton, J. L., Pavia, F. J., Shoenfelt, E. M., & Zhou, Y. (2019) No evidence for equatorial Pacific dust fertilization. *Comment: Nature Geoscience,* 12, 154. https://doi.org/10.1038/s41561-019-0304-z

Katz, M. E., Cramer, B. S., Toggweiler, J. R., Esmay, G., & Wright, J. D. (2011). Impact of Antarctic circumpolar current development on late Paleogene ocean structure. *Science,* 332, 1076–1079.

Katzmann, E., Eibauer, M., Lin, W., Pan, Y., Plitzko, J. M., & Schuler, D. (2013). Analysis of magnetosome chains in magnetotactic bacteria by magnetic measurements and automated image analysis of electron micrographs. *Applied & Environmental Microbiology,* 79, 7755-7762.

Kirschvink, J. L., & Chang, S. R. (1984). Ultrafine-grained magnetite in deep-sea sediments: Possible bacterial magnetofossils. *Geology,* 12, 559-562.

Kopp, R. E., & Kirschvink, J. L. (2008). The identification and biogeochemical interpretation of fossil magnetotactic bacteria. *Earth-Science Reviews,* 86(1–4), 42–61.

Kruiver, P. P., Dekkers, M. J., & Heslop, D. (2001). Quantification of magnetic coercivity components by the analysis of acquisition curves of isothermal remanent magnetization. *Earth and Planetary Science Letters,* 189(3–4), 269–276.

Lascu, I., & Plank, C. (2013). A new dimension to sediment magnetism: Charting the spatial variability of magnetic properties across lake basins. *Global and Planetary Change,* 110, 340–349. https://doi.org/10.1016/j.gloplacha.2013.03.013

Li, J., & Pan, Y. (2012). Environmental factors affect magnetite magnetosome synthesis in Magnetospirillum magneticum AMB-1: implications for biologically controlled mineralization. *Geomicrobiology Journal,* 29, 362–373.

Loveley, M.R., Marcantonio, F., Wisler, M. M., Hertzberg, J. E., Schmidt, M. W., & Lyle, M. (2017). Millennial-scale iron fertilization of the eastern equatorial Pacific over the past 100,000 years. *Nature Geoscience,* 10, 760-64. https://doi.org/10.1038/ngeo3024

Lyle, M. (2008). Bloom without fertilizer. *Nature Geoscience,*1, 576–578.

Marcantonio, F., Hostak, R., Hertzberg, J. E., & Schmidt, M. W. (2020). Deep equatorial Pacific Ocean oxygenation and atmospheric $CO_2$ over the last ice age. *Scientific Reports,* 10(1).

Martin, J. H., (1990). Glacial-interglacial $CO_2$ Change: The Iron Hypothesis. *Paleoceanography,* 5, 1-13. https://doi.org/10.1029/PA005i001p00001

Martinez-Garcia, A., Sigman, D. M., Ren, H., Anderson, R. F., Straub, M., Hodell, D. A., Jaccard, S. L., Eglinton, T. I., & Haug, G. H. (2014). Iron fertilization of the subantarctic ocean during the last ice age. *Science,* 343, 1347–1350.

Murray, R.W., Leinen, M., & Knowlton, C.W. (2012). Links between iron input and opal deposition in the Pleistocene equatorial Pacific Ocean. *Nature Geoscience,* 5, 270-274. https://doi.org/10.1038/ngeo1422

Moore, T. C., Wade, B. S., Westerhold, T., Erhardt, A. M., Coxall, H. K., Baldauf, J., & Wagner, M. (2014). Equatorial Pacific productivity changes near the Eocene-Oligocene boundary, *Paleoceanography,* 29, 825–844. doi:10.1002/ 2014PA002656.

Parés, J. M., & Moore, T. C. (2005). New evidence for the Hawaiian hotspot plume motion since the Eocene. *Earth and Planent Science Letters.* 237, 951–959.

Rae, J. W. B., Zhang, Y. G., Liu, X. Q., Foster, G. L., Stoll, H. M., & Whiteford, R. D. M. (2021). Atmospheric $CO_2$ over the past 66 million years from marine archives. *Annual Review of Earth and Planetary Science,* 49, 609–641.

Rea, D. K., Snoeckx, H. & Joseph, L. H. (1998). Late Cenozoic Eolian deposition in the North Pacific: Asian drying, Tibetan uplift, and cooling of the northern hemisphere. *Paleoceanography,* 13(3), 215-224.

Rippert, N., Max, L., Mackensen, A., Cacho, I., Povea, P., & Tiedemann, R. (2017). Alternating influence of northern versus southern-sourced water masses on the equatorial Pacific subthermocline during the past 240 ka. *Paleoceanography,* 32, 1256-1274. https://doi.org/10.1002/2017PA003133

Roberts, A. P., Pike, C. R., & Verosub, K. L. (2000). First-order reversal curve diagrams: a new tool for characterizing the magnetic properties of natural samples. *Journal of Geophysical Research: Solid Earth,* 105, 28461–28475.

Roberts, A. P., Florindo, F., Villa, G., Chang, L., Jovane, L., Bohaty, S. M., et al. (2011). Magnetotactic bacterial abundance in pelagic marine environments is limited by organic carbon flux and availability of dissolved iron. *Earth and Planetary Science Letters,* 310(3–4), 441–452. https://doi.org/10.1016/j.epsl.2011.08.011

Roberts, A. P., Florindo, F., Chang, L., Heslop, D., Jovane, L., & Larrasoa, A. (2013). Magnetic properties of pelagic marine carbonates. *Earth-Science Reviews,* 127, 111–139.

Rohling, E. J., Yu, J. M., Heslop, D., Foster, G. L., Opdyke, B., & Roberts, A. P. (2021). Sea level and deep-sea temperature reconstructions suggest quasistable states and critical transitions over the past 40 million years. *Science Advances,* 7, eabf5326.

Tagliabue, A., Bowie, A. R., Boyd, P. W., Buck, K. N., Johnson, K. S., & Saito, M. A. (2017). The integral role of iron in ocean biogeochemistry. *Nature,* 543, 51–59.

Takahashi, T., Sutherland, S. C., Wanninkhof, R., Sweeney, C., Feely, R. A., Chipman, D. W., Baar, H. J. W. (2009). Climatological mean and decadal change in surface ocean $pCO_2$, and net sea–air $CO_2$ flux over the global oceans. *Deep Sea Research Part II: Topical Studies in Oceanography,* 56(8-10), 554–577. https://doi.org/10.1016/j.dsr2.2008.12.009

Torres, M.A., West, A.J., & Li, G. (2014). Sulphide oxidation and carbonate dissolution as a source of $CO_2$ over geological timescales. *Nature,* 507, 346–349.

Usui, Y., Yamazaki, T., & Saitoh, M. (2017). Changing abundance of magnetofossil morphologies in pelagic red clay around Minamitorishima, Western North Pacific. *Geochemistry, Geophysics, Geosystems,* 18, 4558–4572. https://doi.org/10.1002/2017GC007127

Westerhold, T., Marwan, N., Deury, A. J., Liebrand, D., Agnini, C., Anagnostou, E., et al. (2020). An astronomically dated record of Earth's climate and its predictability over the last 66 million years. *Science,* 369, 1383–1387.

Winckler, G., Anderson, R.F., Jaccard, S.L., & Marcantonio, F. (2016). Ocean dynamics, not dust, have controlled equatorial Pacific productivity over the past 500,000 years, *Proceedings of the National Academy of Sciences*, 113, 19-24. https://doi.org/10.1073/pnas.1600616113

Yamazaki, T. & Kawahata, H. (1998). Organic carbon flux controls the morphology of magnetofossils in marine sediments. *Geology,* 26, 1064–1066.

Yamazaki, T., Suzuki, Y., Kouduka, M., & Kawamura, N. (2019). Dependence of bacterial magnetosome morphology on chemical conditions in deep-sea sediments. *Earth and Planetary Science Letters,* 513, 135–143. https://doi.org/10.1016/j.epsl.2019.02.015

Yao, W. Q., Markovic, S., Paytan, A., Erhardt, A. M. & Wortmann, U. G. (2021). Quantifying pyrite oxidation on continental shelves during the onset of Antarctic glaciation in the Eocene–Oligocene transition. *Earth and Planetary Science Letters,* 568, 117015.

Zachos, J., Pagani, M., Sloan, L., Thomas, E., & Billups, K. (2001). Trends, rhythms, and aberrations in global climate 65 Ma to present. *Science,* 292, 686–693.

**References from the Supporting Information**

Egli, R. (2013). VARIFORC: an optimized protocol for calculating non-regular first-order reversal curve (FORC) diagrams. *Global and Planetary Change,* 110, 302–320.

Harrison, R. J., & Feinberg, J. M. (2008). FORCinel: an improved algorithm for calculating first-order reversal curve distributions using locally weighted regression smoothing. *Geochemistry, Geophysics, Geosystems,* 9, Q05016.

Lu, Y., Wang, D. F., Jiang, X. D., Lin, Z. Y., Yang, Y. P., & Liu, Q. S. (2021). Paleoenvironmental significance of magnetofossils in pelagic sediments in the equatorial Pacific Ocean before and after the Eocene/Oligocene boundary. Journal of Geophysical Research: Solid Earth, 126, e2021JB022221.

Mortlock, R. A., & Froelich, P. N. (1989). A simple method for the rapid determination of biogenic opal in pelagic marine sediments. *Deep-Sea Research*, 36, 1415–1426.

Taylor, S. R., & Mclennan, S. M. (1985). The continental crust: Its composition and evolution. *Blackwell Scientific,* Oxford.

Westerhold, T., & The Expedition 320/321 Scientists. (2012). Revised composite depth scales and integration of IODP Sites U1331-U1334 and ODP Sites 1218-1220. Proceedings of the Integrated Ocean Drilling Program.

Zhang, Q., Liu, Q., Li, J., & Sun, Y. (2018). An integrated study of the eolian dust in pelagic sediments from the North Pacific Ocean based on environmental magnetism, transmission electron microscopy, and diffuse reflectance spectroscopy. *Journal of Geophysical Research: Solid Earth,* 123:3358–3376.

# Figures

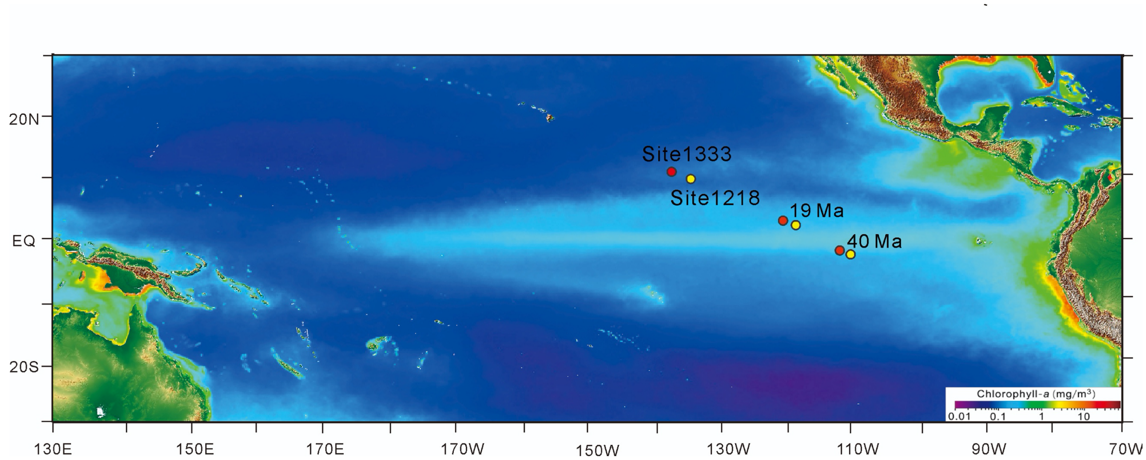


**Figure 1.** Location map. Surface chlorophyll concentration reflects primary production. Palaeo-locations at 40 to 19 Ma are after Parés and Moore (2005). Studied Sites1333 (red circle) and 1218 (yellow circle) was located within the HNLC zone.

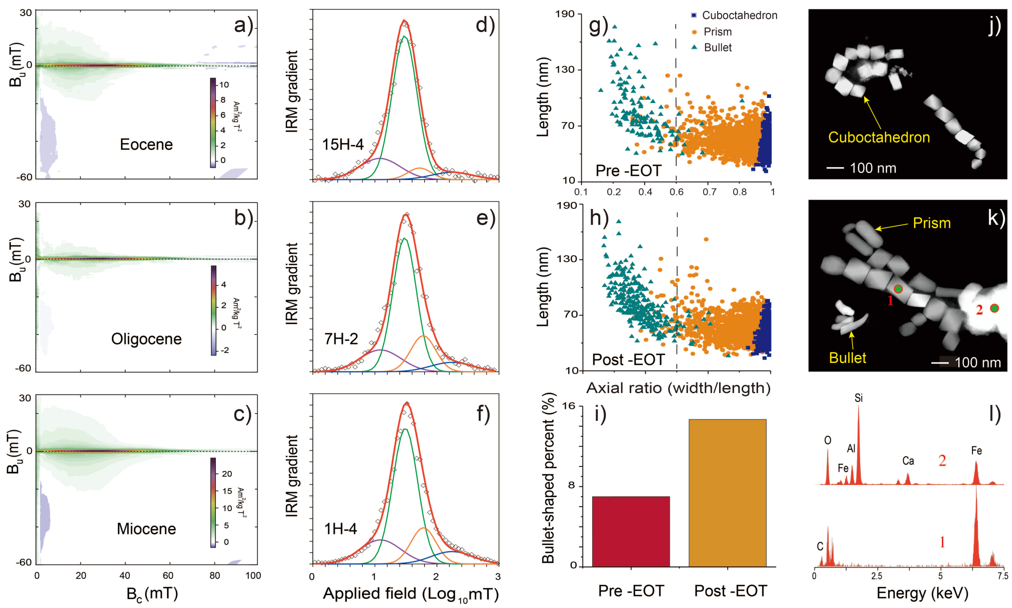


**Figure 2.** Rock magnetic and transmission electron microscope (TEM) results for representative Eocene (15H-4), Oligocene (7H-2), and Miocene (1H-4) samples. (a-c) FORC diagrams with sharp central ridges indicate the domination of non-interacting magnetofossils; (d-f) IRM unmixing results. Open diamonds indicate measured data, fitted components have different colors: red, sum of fitted components; purple (component 1), detrital low-coercivity magnetic assemblages; green (component 2), biogenic soft magnetite; orange (component 3), biogenic hard magnetite; and blue (component 4), detrital high-coercivity magnetic assemblages; (g-k) TEM and statistical analyses of magnetofossil morphologies. Magnetofossils are categorized into high (W/L < 0.6) and lower (0.6 < W/L < 1) anisotropic groups based on shape factor of axial ration; (l) Energy-dispersive X-ray spectroscopy analysis corresponding to the dots in k.

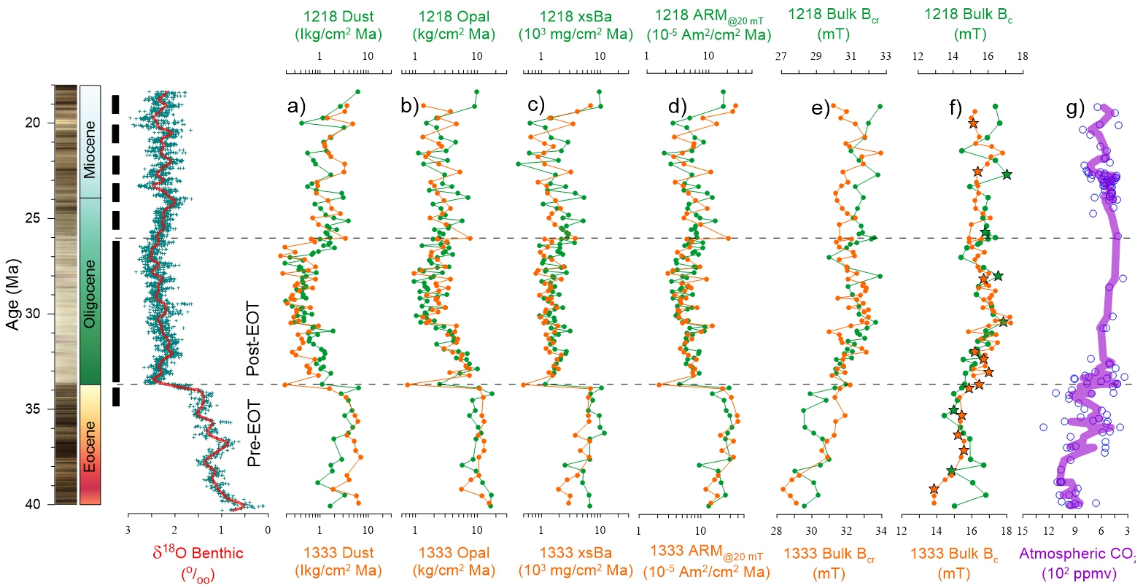


**Figure 3.** Down-core dust, biological productivity (opal, xsBa, ARM$_{@20\ mT}$), $B_{cr}$, and $B_c$ profiles for studied sites. Dashed and solid bars represent periods of small (<50%) and large (>50%) southern hemisphere ice coverage (Zachos et al., 2001). Synchronous benthic foraminiferal $\delta^{18}O$ (Westerhold, et al., 2020) and atmospheric $CO_2$ (Rae et al., 2021) are also shown (solid line = three-point running average). (a-d) Dust stimulated biological pump action provided a negative feedback to the global $CO_2$ changes; (e, f) increased $B_{cr}$ and $B_c$ which reflect the reduction of bottow-water oxygention appeared consistent variations with the later Eocene to early Miocene global $CO_2$ decline. Star symbols in (f) represent samples selected for isothermal remanent magnetization (IRM) unmixing analysis (Supplementary Table S1).

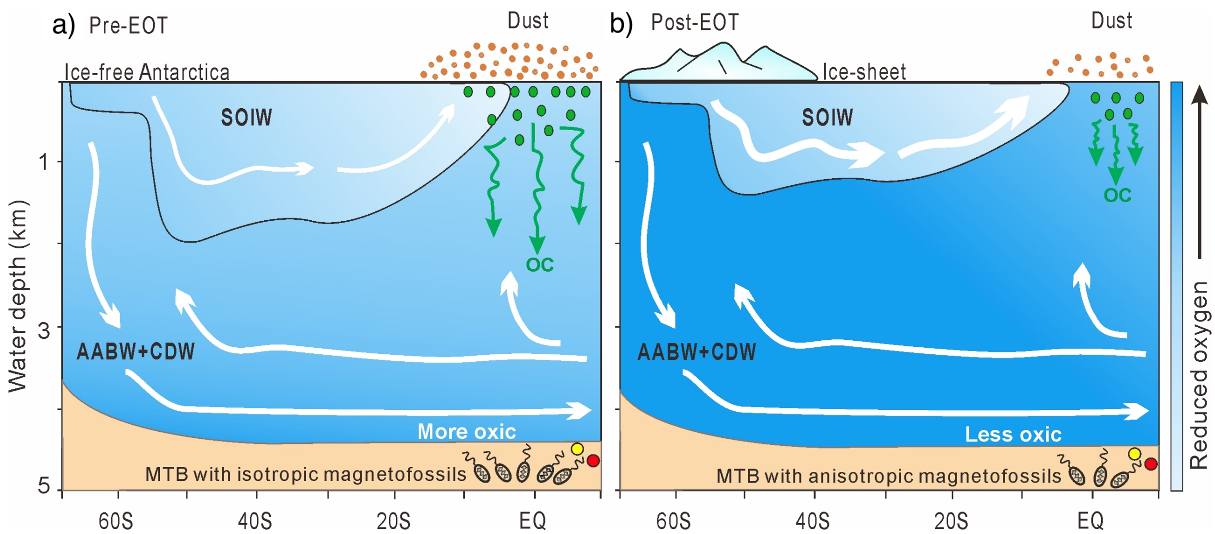


**Figure 4.** Simplified Pacific Ocean meridional hydrography illustrations refer to Rippert et al. (2017) which indicates deep-ocean oxygenation changes across the EOT. General circulation shown as white arrows. Circles indicate location of studied Site 1333 (red) and 1218 (yellow). SOIW, Southern Ocean Intermediate Water. AABW, Antarctic Bottom Water. CDW, Circumpolar Deep Water. OC, Organic Carbon. (a) Pre-EOT, ice-free in Antarctica: more dust stimulated the biological productivity and the bottom-water oxygenation was high; magnetofossil abundance increased whereas the morphological anisotropy reduced. (b) Post-EOT, ice-sheet advanced in Antarctica: large ice cap prevented the air-sea gases exchange and a large amount of bottom-water was formed. Less dust supply reduced the biological productivity and the bottom-water oxygenation was lower; magnetofossil abundance decreased but the morphological anisotropy increased.